Hindawi
Journal of Robotics
Volume 2023, Article ID 8638882, 15 pages
https://doi.org/10.1155/2023/8638882

Research Article

Vector Field-Based Guidance for Planar Smooth Path Following of a Small Unmanned Helicopter

Yang Chen,[1] **Wei Zeng**,[1] **and Yongliang Wu**[2]

[1]*School of Physics and Mechatronics Engineering, Longyan University, Fujian 364000, China*
[2]*Department of Mechanics and Aerospace Engineering, Southern University of Science and Technology, Shenzhen 518055, China*

Correspondence should be addressed to Yang Chen; chenyang4117@163.com

Received 2 July 2022; Revised 27 August 2022; Accepted 28 April 2023; Published 11 May 2023

Academic Editor: Shuofei Yang

This study investigates a guidance method that will allow the small unmanned helicopter to follow the predefined horizontal smooth path. A stable nonlinear guidance law, which needs the information of the inertial position and groundspeed of the helicopter and the implicit function of the desired path, is designed to generate the reference course rate command based on the concept of the vector field. The asymptotic approximation to the desired path with bounded following errors has also been demonstrated by using the Lyapunov stability arguments. Some conditions for guaranteeing the stability have been extended. Simulations on following four types of planar paths, i.e., the square, circular, elliptic, and cubic curve paths, have verified the effectiveness of the proposed method. The predefined square path following performance of the proposed vector field-based method is compared with another two guidance laws, which are based on the PD-like and fuzzy logic control. The comparison shows that the proposed method can guide the helicopter to follow the predefined path most smoothly. The maximum overshoot by using the proposed method is less than 0.016 meters, while those by using the other two methods are all larger than 0.80 meters. Moreover, the vector field-based method will cost the least time for the vehicle to converge to the predefined path.

1. Introduction

Small unmanned aerial vehicles including the fixed-wing [1], quadrotors [2], and helicopter [3] have been studied and applied in military and civilian fields in past decades. The unmanned helicopters have attracted many researchers because they can fly vertically and manoeuvre in narrow spaces, especially hovering over interesting areas [3], such as the scene of the residential structure fire, the high-voltage transmission tower, and the damage position of the bridge. In the aspects of research, the vision-aided navigation and control of unmanned helicopters [4, 5], conflict-free navigation [6], monocular vision based indoor flight [7], and cooperative control of multiple unmanned helicopters [8] have appeared in recent years. It needs the vehicle to have the ability to follow (or track) the predefined path (or trajectory) precisely to realize the autonomous or automatic control of its own.

According to the model-based controller structure, the approaches to realize the path following or trajectory tracking control of a small unmanned helicopter can be divided into two main categories. One approach uses an integrated method to solve the helicopter's guidance and control problem simultaneously. The alternative method adopts the hierarchical control architecture to separate the above problem into an inner loop for stabilizing its dynamics and an outer loop for guidance.

The integrated method to realize the path following or trajectory tracking mostly appears on the nonlinear control techniques. Zhou et al. applied the concept of backstepping control for the helicopter in continuous time [9] to track the predefined position and yaw reference trajectories. Razzaghian and Kardehi Moghaddam applied the nonlinear fuzzy sliding mode control method to the trajectory control of the helicopter with the help of a dynamic inverter [10]. Tsai et al. combined the fuzzy basis function networks and the

backstepping technique to reach the design of an intelligent adaptive tracking controller, where its performance was also compared with a numerical neural network controller [11, 12]. Benitez-Morales et al. [13] applied the feedback linearization control methodology for the trajectory tracking of a small helicopter's nonlinear longitudinal dynamics in simulation. Kim and Shim used the nonlinear model predictive control (MPC) method to track the predefined trajectory where the nonlinear model contains the kinematics and the system specific dynamics [14]. The application of the MPC method for realizing the path tracking in unknown and cluttered environments was also discussed in [15]. While applying the nonlinear control methods, it needs good knowledge of the vehicle's nonlinear model. Furthermore, the backstepping and fuzzy technique will mostly introduce new parameters and transformed variables. The computation of the neural network and model predictive control is large. All of the above make them difficult to be used in the low-cost avionics systems.

While applying the separate inner and outer loop approach, the inner loop control usually uses the simple and well-established design methods. For guidance design, the traditional proportion integration differentiation (PID) controllers are used due to its simple structure and effectiveness [16, 17]. And it is mostly used in the lateral/longitudinal manoeuvres by reducing the lateral deviation from a desired fight path. Two Mamdani-type fuzzy controllers were used to handle the lateral/longitudinal control, respectively, in [18]. The robust control techniques have also been applied in the guidance loop design. A Kalman-filter based linear quadratic integral (LQI) controller was used for the position controller design by considering the characteristics of the inner attitude closed-loop dynamics [19]. Bergerman et al. adopted the FLC method together with the simple PD controller for the position and heading control of a helicopter [20]. The authors of reference [21] developed a composite nonlinear feedback control technique to achieve a high-performance position control. Part of the technique is based on the linear $H_2/H\infty$ optimization method. The robust control techniques are useful for the outer loop design. However, it needs much more calculation due to its higher order compared with the simple PID technique. Marantos et al. proposed a robust control scheme that is decomposed into a position and an attitude control module, operating in a cascaded form with low complexity [22]. Ma and Huo applied the hierarchical inner-outer loop structure to realize the singularity-free path following control of an unmanned helicopter. The outer-loop position controller is constructed with the hyperbolic tangent function [23].

Considering the controller structure and the purpose of the horizontal path following of a small unmanned helicopter with low-cost avionics, we adopted the hierarchical control architecture for the flight control system design. The unstable dynamics of the helicopter have been stabilized by the setpoint tracking LQG control technique [24]. The LQG technique can also track the reference heading rate and velocities in the body-fixed coordinate frame.

The core part of the outer loop is based on the concept of the vector field which has been successfully applied in miniature aerial vehicles to generate the commanded course rate [25]. The method calculates a vector field around the path to be followed. The vectors in the field are directed toward the path to be followed and represent the desired direction of flight. And it has realized the waypoint path following and collision avoidance for the vehicles in the simulation and real flight tests [26, 27]. In [25], the straight-line and circular orbit paths following approaches have been provided. However, in some cases, the route of an aircraft is a more complex smooth curve. In order to follow the general horizontal smooth paths that can be expressed by implicit functions, including the ellipse and cubic curve, a general smooth path following guidance law based on the concept of the vector field has been produced for a small unmanned helicopter in this study.

The main contributions of this study are summarized as follows: First, a guidance law based on the vector field for following a class of horizontal paths is presented in the Cartesian coordinate system. The stability of the path following with bounded following errors is demonstrated by the Lyapunov stability arguments. Second, some conditions for guaranteeing the stability have been extended by comparing with those appeared in [24]. The simulations about tracking the square, quadratic, and cubic curves were presented to evaluate the effectiveness of proposed method. The following performance of the square path was compared with those by using another tow guidance laws. Third, the control results were compared with another two guidance laws based on the PD-like and fuzzy logic control, which illustrates the effectiveness and better performance of the proposed control strategies.

The remainder of the paper is organized as follows: The formal problem description for a small unmanned helicopter to follow a predefined smooth path was given in Section 2. In Section 3, the course rate command is generated based on the concept of the vector field. The detailed stability analysis is also given. In Section 4, the simulation details on four types of planar paths are presented. The conclusion and future work are given in Section 5.

2. Problem Description

The helicopter adopts the hierarchical control architecture for the planar smooth path following. Figure 1 shows the structure of the control system. The inner-loop controller is used not only to stabilize the helicopter dynamics but also track the reference signals from outputs of the outer-loop controller. The outer-loop controller design is based on the inertial positions and velocity of the helicopter and the desired path from the path generator. And it is used to generate the desired heading rate and velocities.

In Figure 1, $[p_N^I, p_E^I, p_D^I]$ denotes the position of the center of gravity of the helicopter in the local north-east-down, Cartesian coordinates [20]. u_{ref}, v_{ref}, w_{ref}, and r_{ref} denote the reference velocities and the heading rate in the body-fixed coordinates, respectively.

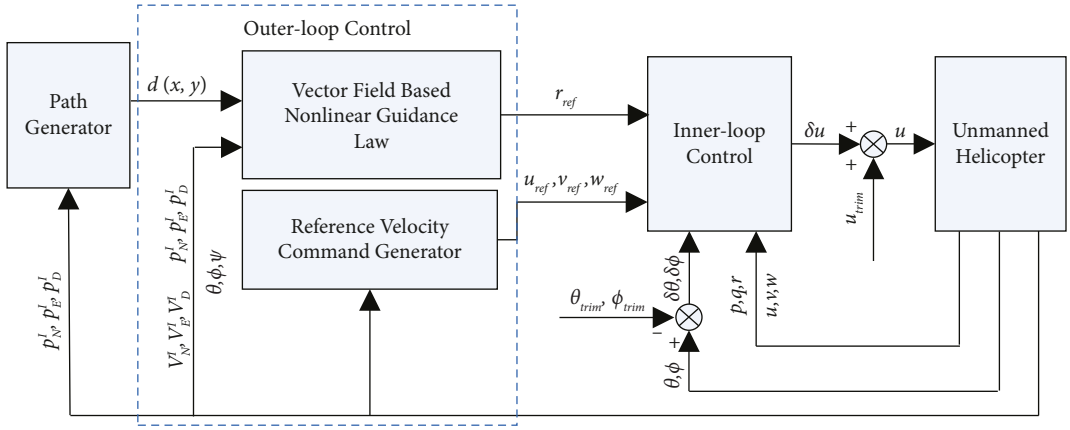

Figure 1: The hierarchical flight control structure for the helicopter.

The design of the inner-loop controller is based on the helicopter's dynamics. And a setpoint LQG technique [24] with the combination of an LQR and a linear quadratic estimator is used not only to stabilize the internal stability of the unmanned helicopter but also to track the reference signals u_{ref}, v_{ref}, w_{ref}, and r_{ref}.

The outer-loop controller design is separated into two parts which are used to produce the reference velocities and the heading rate command, respectively. The vertical reference velocity design is based on the PI method. In this paper, we only consider the reference heading rate command generator. The following two assumptions are adopted:

Assumption 1. The set altitude of the helicopter was well controlled. It means that the flight path of the vehicle is on the horizontal plane with a certain height in the local coordinate system.

Assumption 2. The heading of the flying vehicle ψ is assumed to be equal to its course χ (see Figure 2). If the helicopter is working in the low-speed flight mode, it has $\dot{\psi} \approx r$ [20]. Then, the reference heading rate r_{ref} can be generated as the course rate command u_{cmd} shown in (2), i.e., $r_{\text{ref}} = u_{\text{cmd}}$.

In this study, the desired horizontal smooth path is presented by a twice continuously differentiable implicit function $f: R^2 \longrightarrow R$ as follows:

$$f(x, y) = 0, \tag{1}$$

where $x = p_N^I$ and $y = p_E^I$. To generate the heading (course) rate command, the kinematics of the helicopter in the inertial north-east frame is used, and it is given as follows:

$$\begin{cases} \dot{x} = V_g \cos(\chi), \\ \dot{y} = V_g \sin(\chi), \\ \dot{\chi} = u_{\text{cmd}}, \end{cases} \tag{2}$$

where the groundspeed $V_g \in [V_{g,\min}, V_{g,\max}]$. $V_{g,\min}$ and $V_{g,\max}$ are positive constants.

Considering that the desired path (1) is the generic curve, it is difficult to express the explicit Euclidean distance between the position of the helicopter and the generic curve-based path mostly. The value $f(x, y)$ when the UAV is in (x, y) is used as the distance value. In this study, the nominal distance function $d(x, y)$ is defined as $d(x, y) = f(x, y)$. The value of $d(x, y)$ can represent the position of the helicopter relative to the desired path. If $d(x, y) = 0$, it means that the helicopter is on the path. Moreover, it can distinguish whether the helicopter is within the curve when the curve is closed or the helicopter is on the right half-plane of the curve when the curve is not closed.

The following is to design the heading (course) rate command u_{cmd} which will make the helicopter fly along the desired path in the right direction.

3. Vector Field-Based Nonlinear Guidance Law

The magnitude gradient of $d(x, y)$ in point (x, y) is denoted as $\|\nabla f\| = \sqrt{f_x^2 + f_y^2}$, where f_x and f_y are the partial derivatives of $d(x, y)$ or $f(x, y)$) with respect to x and y, respectively. For some given $f(x, y)$, the value of $\|\nabla f\|$ may be zero in some points (x, y). If the helicopter's initial position is at these points, the guidance to be designed below will fail, and the helicopter will lose control. In order to avoid the helicopter being trapped at the center point of the closed curve (such as the center of a circle or ellipse), the flight domain for the helicopter is defined as $D_{\text{int}} = \{x, y | x, y \in R, \|\nabla f\| \geq \lambda\}$, where $\lambda > 0$ defines the size of the no-fly zone.

The desired course is defined as follows:

$$\chi_d(d(x, y)) = g(d(x, y)) + \xi(x, y), \tag{3}$$

where $g(x)$ is a C^2 odd function which is strictly monotonic increasing over $(-\infty, +\infty)$ with $-\pi/2 < g(x) < \pi/2$ for all x. Another property of $g(x)$ is that its derivative, i.e., $g'(x)$, is monotonic decreasing over $[0, +\infty]$. Then, it has the fact that $g'(x)$ is monotonic increasing over $[-\infty, 0]$, $g(0) = 0$, and

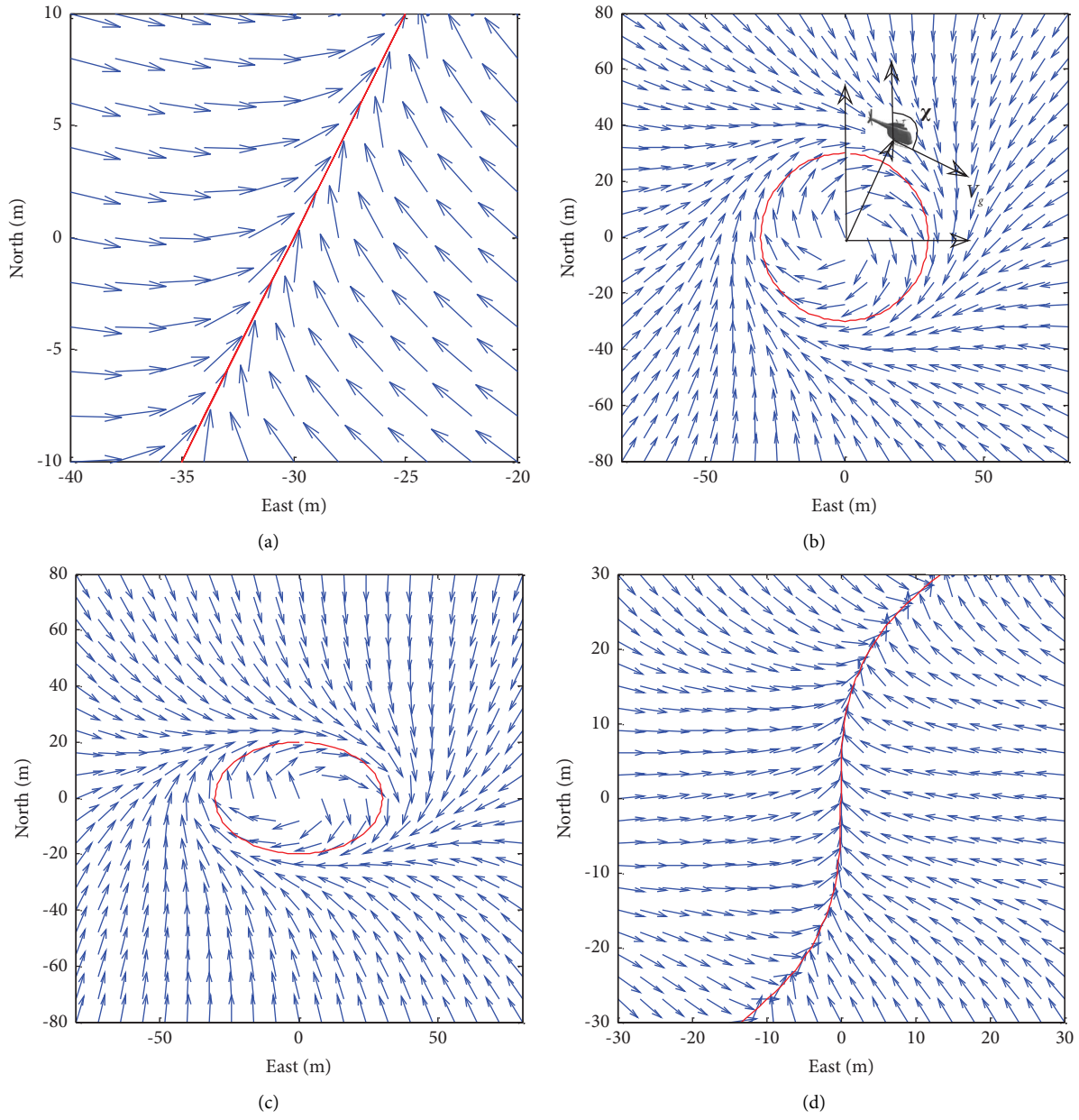

Figure 2: The vector field for path following (a) straight-line, (b) circle, (c) ellipse, and (d) cubic curve.

$xg(x) > 0$ for $x \neq 0$. $\xi(x, y)$ is defined as $\xi(x, y) = \mathrm{mod}(\mathrm{atan}\,2(f_x, -f_y), 2\pi)$, and it has the fact that

$$\begin{cases} \sin(\xi(x, y)) = \dfrac{f_x}{\|\nabla f\|}, \\ \\ \cos(\xi(x, y)) = -\dfrac{f_y}{\|\nabla f\|}. \end{cases} \tag{4}$$

The desired course shown in (3) has two parts: $g(d(x, y))$ and $\xi(x, y)$. If the helicopter is on the desired path $f(x, y) = 0$, then $g(d(x, y)) = g(0) = 0$, and $\xi(x, y)$ is the tangent direction of the desired path. If the helicopter is far away from the desired path, then $g(d(x, y)) \longrightarrow \pm \pi/2$. Together with the property of $g'(x)$, the desired course is to guide the helicopter approach the desired path with the course angle from $\pm \pi/2 + \xi(x, y)$ to $\xi(x, y)$. For example, if the helicopter is far away from a desired straight-line path, then $\xi(x, y) = 0$. In this case, the desired course is $\pm \pi/2$, which is to make the helicopter fly vertically to the desired straight-line path.

Figure 2 shows the corresponding vector field derived from (1)–(3), where the curve is straight line, circle, ellipse, and cubic curve, respectively. The ground velocity in the horizontal plane is chosen as $V_g = 3m/s$. The function $g(x)$ in (3) is chosen as $g(x) = \mathrm{atan}(k_1 x)$ with $k_1 = 0.4$. The implicit functions of the straight line, circular, elliptic, and cubic curve paths in Figure 2 are $x - 2y - 60 = 0$, $x^2/900 + y^2/900 - 1 = 0$, $x^2/400 + y^2/900 - 1 = 0$, and $0.0005x^3 - y = 0$, respectively. The goal is that the helicopter

can follow the vector towards the desired path at its current position.

The state variables are defined as $(d(x,y),\tilde{\chi})^T$, where $\tilde{\chi}=\chi-\chi_d$. The dynamics of the variables can be derived as follows:

$$\begin{aligned}\dot{d}(x,y) &= f_x\dot{x}+f_y\dot{y},\\ &= f_xV_g\cos(\chi)+f_yV_g\sin(\chi),\\ &= V_g\|\nabla f\|\left(\frac{f_x}{\|\nabla f\|}\cos(\chi)+\frac{f_y}{\|\nabla f\|}\sin(\chi)\right),\\ &= V_g\|\nabla f\|(\sin(\xi(x,y))\cos(\chi)\\ &\quad-\cos(\xi(x,y))\sin(\chi)),\\ &= -V_g\|\nabla f\|\sin(\chi-\xi(x,y)),\\ &= -V_g\|\nabla f\|\sin(\tilde{\chi}+g(d(x,y))),\\ \dot{\tilde{\chi}} &= \dot{\chi}-\dot{\chi}_d=u_{\text{cmd}}-\dot{\chi}_d.\end{aligned}\tag{5}$$

The main purpose of this study is to find the course rate command u_{cmd}, which will make the errors $d(x,y)$ and $\tilde{\chi}$ converge to zeros as the time goes to infinity, i.e., make the helicopter fly along the desired path with bounded errors in finite time.

Theorem 1. *If the flying helicopter's initial position is not on the desired path but within the flight domain D_{int}, the course rate command shown as (6), which is a nonlinear combination of the course error $\tilde{\chi}$ and the time derivative of the desired course shown as (3), will make the helicopter approach the desired path with the desired course and fly along the desired path with bounded errors in finite time.*

$$\begin{aligned}u_{\text{cmd}} &= -k\|\nabla f\|\text{sat}\left(\frac{\tilde{\chi}}{\varepsilon}\right)+\frac{d}{dt}\chi_d(d(x,y)),\\ &= -k\|\nabla f\|\text{sat}\left(\frac{\tilde{\chi}}{\varepsilon}\right)\\ &\quad+g'(d(x,y))\frac{d}{dt}d(x,y)+\frac{d}{dt}\xi(x,y),\end{aligned}\tag{6}$$

where $k>0$ and $\varepsilon>0$. The parameters satisfy the following conditions: $\varepsilon<\mu_2<\mu_1\bar{d}/2$, $\varepsilon V_{g,\max}/2k\rho<\mu_1<\cos(g(\bar{d}))g'(\bar{d})$, and $\mu_2<\sin(g(\bar{d}))$ with $\rho>0$, and the positive value $\bar{d}$ is arbitrary chosen. The conditions are different with those in [24]. The saturation function $\text{sat}(x)$ is defined as follows:

$$\text{sat}(x)=\begin{cases}1, & x>1,\\ x, & -1\le x\le 1,\\ -1, & x<-1.\end{cases}\tag{7}$$

Proof. Substitute u_{cmd} shown as (6) into (5), then

$$\begin{cases}\dot{d}(x,y)=-V_g\|\nabla f\|\sin(\tilde{\chi}+g(d(x,y))),\\ \dot{\tilde{\chi}}=-k\|\nabla f\|\text{sat}\left(\frac{\tilde{\chi}}{\varepsilon}\right).\end{cases}\tag{8}$$

It can be found that the equilibrium point of the nonlinear system (8) is $(0,0)^T$.

Let $W_1=\tilde{\chi}^2/2$, and the boundary region around the sliding surface with respect to ε is defined as $S_\varepsilon=\{|\tilde{\chi}|\le\varepsilon\}$. Then, the derivative of W_1 is as follows:

$$\dot{W}_1=\tilde{\chi}\dot{\tilde{\chi}}=-k\|\nabla f\|\tilde{\chi}\text{sat}\left(\frac{\tilde{\chi}}{\varepsilon}\right).\tag{9}$$

So, if $|\tilde{\chi}|\ge\varepsilon$, then $\dot{W}_1=-k\|\nabla f\||\tilde{\chi}|\le-k\lambda\varepsilon$, and it gets that $\tilde{\chi}$ will reach S_ε in finite time. It remains to show that, inside S_ε, system (8) will converge to the equilibrium point $(0,0)^T$. The Lyapunov candidate function is defined as follows:

$$W=\frac{1}{2}d^2(x,y)+\frac{1}{2}\rho\tilde{\chi}^2.\tag{10}$$

Differentiating W with respect to time, it has

$$\begin{aligned}\dot{W} &= d(x,y)\dot{d}(x,y)+\rho\tilde{\chi}\dot{\tilde{\chi}}\\ &= -V_g\|\nabla f\|\sin(\tilde{\chi}+g(d(x,y))),\\ &\quad-\rho k\|\nabla f\|\tilde{\chi}\text{sat}\left(\frac{\tilde{\chi}}{\varepsilon}\right).\end{aligned}\tag{11}$$

Inside the boundary region S_ε, it has $|\tilde{\chi}|\le\varepsilon$. So,

$$\begin{aligned}\dot{W} &= -V_g\|\nabla f\|\sin(\tilde{\chi}+g(d(x,y)))-\|\nabla f\|\frac{k\rho}{\varepsilon}\tilde{\chi}^2\\ &= -\|\nabla f\|\frac{k\rho}{\varepsilon}\tilde{\chi}^2-d(x,y)V_g\|\nabla f\|\sin(g(d(x,y)))\\ &\quad+d(x,y)V_g\|\nabla f\|(\sin(g(d(x,y)))\\ &\quad-\sin(\tilde{\chi}+g(d(x,y))))\\ &= \|\nabla f\|\left(-\frac{k\rho}{\varepsilon}\tilde{\chi}^2-d(x,y)V_g\sin(g(d(x,y)))\right)\\ &\quad-2d(x,y)V_g\|\nabla f\|\sin\left(\frac{\tilde{\chi}}{2}\right)\cos\left(g(d(x,y))+\frac{\tilde{\chi}}{2}\right)\\ &\le \|\nabla f\|\left(-\frac{k\rho}{\varepsilon}\tilde{\chi}^2-d(x,y)V_g\sin(g(d(x,y)))\right)\\ &\quad+2|d(x,y)|V_g\|\nabla f\|\left|\frac{\tilde{\chi}}{2}\right|,\\ &= \|\nabla f\|\left(-\frac{k\rho}{\varepsilon}\tilde{\chi}^2-d(x,y)V_g\sin(g(d(x,y)))\right.\\ &\quad\left.+2|d(x,y)|V_g\left|\frac{\tilde{\chi}}{2}\right|\right).\end{aligned}\tag{12}$$

Let $(x)=x\sin(g(x))$, and

$$\xi(x) = \begin{cases} \dfrac{\mu_1 x^2}{2}, \text{if} |x| \le \overline{d}, \\ \\ \mu_2 (|x| - \overline{d}) + \dfrac{\mu_1 \overline{d}^2}{2}, if |x| > \overline{d}, \end{cases} \tag{13}$$

where $\mu_1 > 0$, $\mu_2 > 0$, and $\overline{d}$ is arbitrary. It has the fact that both $\phi(x)$ and $\xi(x)$ are symmetric functions in x, and $\phi(0) = \xi(0) = 0$. It is noted that the function $\xi(x)$ defined here is different from that appeared in [24], which will extend the condition for the stability.

When $0 \le x \le \overline{d}$, then $\xi^{'}(x) = \mu_1 x$, and

$$\begin{aligned} \phi^{'}(x) &= x \cos(g(x)) g^{'}(x) + \sin(g(x)), \\ &\ge x \cos(g(x)) g^{'}(x), \\ &\ge x \cos(g(\overline{d})) g^{'}(\overline{d}). \end{aligned} \tag{14}$$

If $\mu_1 < \cos(g(\overline{d})) g^{'}(\overline{d})$, then $\phi^{'}(x) \ge \xi^{'}(x)$.

When $\overline{d} \le x$, then $\xi^{'}(x) = \mu_2$ and $\phi(x) = x \sin(g(x)) \ge x \sin(g(\overline{d}))$. If $\mu_2 \le \sin(g(\overline{d}))$, it derives that $\phi^{'}(x) \ge \xi^{'}(x)$. So while $\mu_1 < \cos(g(\overline{d})) g^{'}(\overline{d})$ and $\mu_2 \le \sin(g(\overline{d}))$, then $\phi(x) \ge \xi(x)$ for x in $(-\infty, +\infty)$.

Figure 3 shows the plot comparison of the function $\phi(x)$ and $\xi(x)$ with $g(x) = \text{atan}(0.4x)$, $\overline{d} = 2$, and $\mu_1 = 0.18$. The blue solid line is the plot of function $\phi(x)$ with respect to x. The red dashed line is the plot of function $\xi(x)$ as shown in [24]. The black dotted line is the plot of one of feasible functions $\xi(x)$ with $\mu_2 = 0.155$ in this paper. In fact, $\phi(x) \ge \xi(x)$, and the function $\xi(x)$ in [24] is the special case of (13).

Furthermore, if $\varepsilon < \mu_2 < \mu_1 \overline{d}/2$ and $\varepsilon V_{g,\max} < 2k\rho\mu_1$, when $\overline{d} \le |d(x, y)|$, then

$$\begin{aligned} \dot{W} &\le \|\nabla f\| \left(-V_g \left(\mu_2 (|d(x, y)| - \overline{d}) + \frac{\mu_1 \overline{d}^2}{2} \right) \right. \\ &\quad \left. - \frac{k\rho}{\varepsilon} \tilde{\chi}^2 + V_g |d(x, y)| |\tilde{\chi}| \right) \\ &= -\frac{k\rho}{\varepsilon} \|\nabla f\| \tilde{\chi}^2 + V_g \|\nabla f\| \left(-\mu_2 |d(x, y)| \right. \\ &\quad \left. + \left(\mu_2 - \frac{\mu_1 \overline{d}}{2} \right) \overline{d} + |d(x, y)| |\tilde{\chi}| \right) \\ &\le V_g \|\nabla f\| \left(-\mu_2 |d(x, y)| + |d(x, y)| |\tilde{\chi}| \right) \\ &\le V_g \|\nabla f\| \left(-\mu_2 |d(x, y)| + |d(x, y)| \varepsilon \right) \\ &= -V_g \|\nabla f\| |d(x, y)| (\mu_2 - \varepsilon) \\ &\le -V_{g,\min} \lambda |d(x, y)| (\mu_2 - \varepsilon) \\ &= -V_{g,\min} \lambda \overline{d} (\mu_2 - \varepsilon) < 0. \end{aligned} \tag{15}$$

It derives that, when $\overline{d} \le |d(x, y)|$, the control law (6) will make $d(x, y)$ reach $\overline{d}$ in finite time.

When $|d(x, y)| \le \overline{d}$, then

$$\begin{aligned} \dot{W} &\le \|\nabla f\| \left(-\frac{k\rho}{\varepsilon} \tilde{\chi}^2 - V_g \frac{\mu_1 d^2(x, y)}{2} + V_g |d(x, y)| |\tilde{\chi}| \right) \\ &= \|\nabla f\| V_g \left(-\frac{k\rho}{\varepsilon V_g} \tilde{\chi}^2 - \frac{\mu_1 d^2(x, y)}{2} + |d(x, y)| |\tilde{\chi}| \right) \\ &\le \|\nabla f\| V_g \left(-\frac{k\rho}{\varepsilon V_{g,\max}} \tilde{\chi}^2 - \frac{\mu_1 d^2(x, y)}{2} + |d(x, y)| |\tilde{\chi}| \right) \\ &= -\|\nabla f\| V_g (|d(x, y)|, |\tilde{\chi}|) \mathbf{M} (|d(x, y)|, |\tilde{\chi}|)^T \\ &\le -\lambda V_{g,\min} (|d(x, y)|, |\tilde{\chi}|) \mathbf{M} (|d(x, y)|, |\tilde{\chi}|)^T \\ &= -W_3 (d(x, y), \tilde{\chi}), \end{aligned} \tag{16}$$

where the matrix $\mathbf{M} = \begin{bmatrix} \mu_1/2 & -1/2 \\ -1/2 & k\rho/\varepsilon V_{g,\max} \end{bmatrix}$ is positive definite. It has the fact that the function $W_3(d(x, y), \tilde{\chi})$ is continuous positive definite. Then, it derives that the equilibrium point of the nonlinear system (8) is uniformly asymptotically stable [28].

Thus, if $\varepsilon < \mu_2 < \mu_1 \overline{d}/2$, $\mu_2 < \sin(g(\overline{d}))$, and $\varepsilon V_{g,\max}/2k\rho < \mu_1 < \cos(g(\overline{d})) g^{'}(\overline{d})$, $\mu_2 \le \sin(g(\overline{d}))$ with the arbitrary chosen value $\overline{d}$. It can state that the control law (6) will make the helicopter fly along the desired path with bounded errors in finite time. And the path following errors (the distance and course error) will converge to zeros as the time goes to infinity. □

4. Simulations

This section presents the simulations of the proposed vector field-based guidance law for the path following of an ALIGN T-Rex 600 RC model helicopter (see Figure 4). The helicopter was instrumented with avionics weights 4.9 kg. For simulation, the detailed inner-loop controller design together with the linear model of the helicopter can be seen in [24]. And we choose $g(x) = \text{atan}(0.4x)$, $k = \pi/2$, and $\varepsilon = 0.15$, respectively. The local earth-fixed coordinate system is defined to follow the north-east-down convention. The forward and sideway reference velocities along the body axis of the helicopter were set as $u_{\text{ref}} = 3m/s$ and $v_{\text{ref}} = 0m/s$, respectively. The simulation sample time was set as 20 ms.

While conducting the simulations, we applied the proposed method to follow four types of planar paths, i.e., the square, circular, elliptic, and cubic curve paths in the Matlab/Simulink GUI environment, respectively. The helicopter flied in a counter clockwise direction.

4.1. Square Path Following. In this section, another two guidance laws have also been applied to follow the square path. The results will be compared to show the performance of the proposed vector field-based method. The first one for comparison is a PD-like nonlinear control law (PD_PFC) [29] shown as follows:

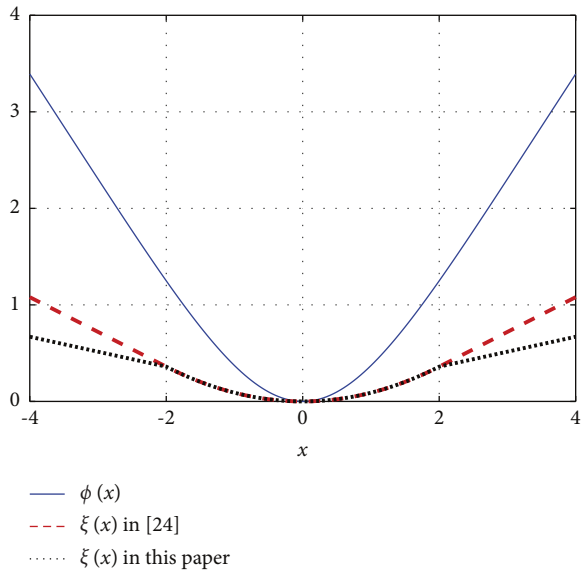

Figure 3: The plot comparison of $\phi(x)$ and $\xi(x)$.

$$u_{\text{cmd}} = -K_1 V_g f_{\text{sat}}(D(x, y)) - K_2 V_g \frac{dD(x, y)}{dt}, \quad (17)$$

where K_1 and K_2 are the constant parameters, and the signed value $D(x, y)$ denotes the vertical distance from the current position of the vehicle to the desired straight line.

The other guidance law has the same expression as PD_PFC, but the parameter K_2 is adjusted by the fuzzy logic (FC_PFC). The structure of the FC_PFC is shown in Figure 5, and the control parameter K_2 is given as follows:

$$k_2 = k_{20} + \Delta k_2, \quad (18)$$

where K_{20} is a constant, and Δk_2 is the tuning part for k_2. In the design of fuzzy control logic, the domains of discourse for the two inputs ($D(x, y)$ and $\dot{D}(x, y)$) and the output Δk_2 are set as $[-6, 6]$, $[-3, 3]$, and $[-0.09, 0.09]$, respectively. The details of the membership functions and the rules for the design of the fuzzy logic unit can be seen in [29]. In this study, we choose $K_1 = 0.05$ and $K_{20} = 0.075$, respectively. Then, $K_2 > 0.018$, according to the fuzzy control mechanism shown in [29]. In this case, the control law shown FC_PFC can make the helicopter fly along the predefined straight-line path.

The initial position of the small unmanned helicopter was set as (5, 40, −20) in the local north-east-down frame, and its initial heading was set as 90° east. The predefined square path has four waypoints, (A (0, 0, −20), B (0, 80, −20), C (80, 0, −20), and D (80, 80, −20)), as shown in Figure 6(a). Figure 6(b) shows the path following comparison with the three methods, PD_PFC, FC_PFC, and the vector field in the horizontal plane.

Figure 7 shows the comparison of the deviation $D(x, y)$ when the helicopter follows the square path with the methods PD_PFC, FC_PFC, and the vector field. While doing the waypoint switch, the helicopter will switch route if the distance between the position of the vehicle and the next waypoint is less than 8 m. This mechanism causes the abrupt

Figure 4: The model unmanned helicopter for simulation.

changes of $D(x, y)$ with about 8 meters. Figure 7 also shows that the proposed vector field method will make the helicopter reach much smoother transition of course with smaller overshoot and oscillation amplitude of $D(x, y)$ than those by using the other two methods, PD_PFC and FC_PFC.

Figure 8 shows the comparison of the course rate command u_{cmd} with the methods PD_PFC, FC_PFC, and the vector field. When the route is switched, compared with the other two methods, PD_PFC and FC_PFC, the course rate command u_{cmd} generated by using the method vector field can converge to zero most quickly, which means that the method can make the helicopter fly along the target route most quickly. Figures 9 and 10 show the $g(d(x, y))$ and $\xi(x, y)$ in (3) while following the predefined square path. The corresponding value ranges are (0, 1.27) and (0, 4.71), respectively.

Table 1 presents the comparison of the maximum overshoots, rise time, and convergence time displayed in the elliptic areas, (a), (b), (c), (d), (e), and (f) of Figure 7. The rise time refers to the length of time that the helicopter flies toward the straight line before $|D(x, y)|$ the first time becomes less than 0.4 meters. The convergence time is defined as the time from the helicopter following the desired path until $|D(x, y)|$ is less than 0.4 meters. It can be seen that the maximum overshoot by using the method vector field is less than 0.016 meters, while that by using the method FC_PFC is within the range of 0.81~0.87 meters. The maximum overshoot produced by using the method PD_PFC is about 1.9 meters, which is the largest. The method PD_PFC has the shortest rise time, which is about 2.64 s. While using the methods, the vector field and FC_PFC, the corresponding rise times are about 3.66 s and 3.5 s, respectively. However, the convergence times by using the method vector field are all less than 3.72 s. The corresponding convergence times by using the methods FC_PFC and PD_PFC are all lager than 7.30 s.

Table 2 shows the average and the standard deviation values of the distance $D(x, y)$ of the three methods, respectively. The comparison of the standard deviation values and the maximum overshoots show that the vector field method makes the helicopter to follow the predefined path most smoothly. The mean value of $D(x, y)$ by using the

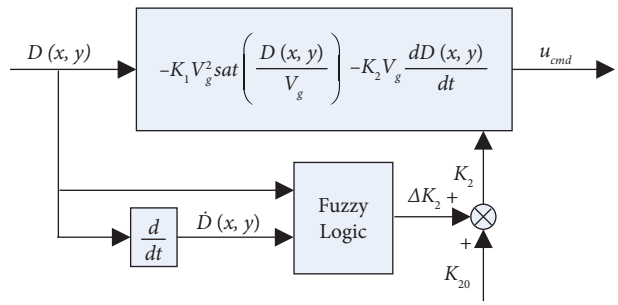

Figure 5: The structure of the FC_PFC course rate command generator for the helicopter.

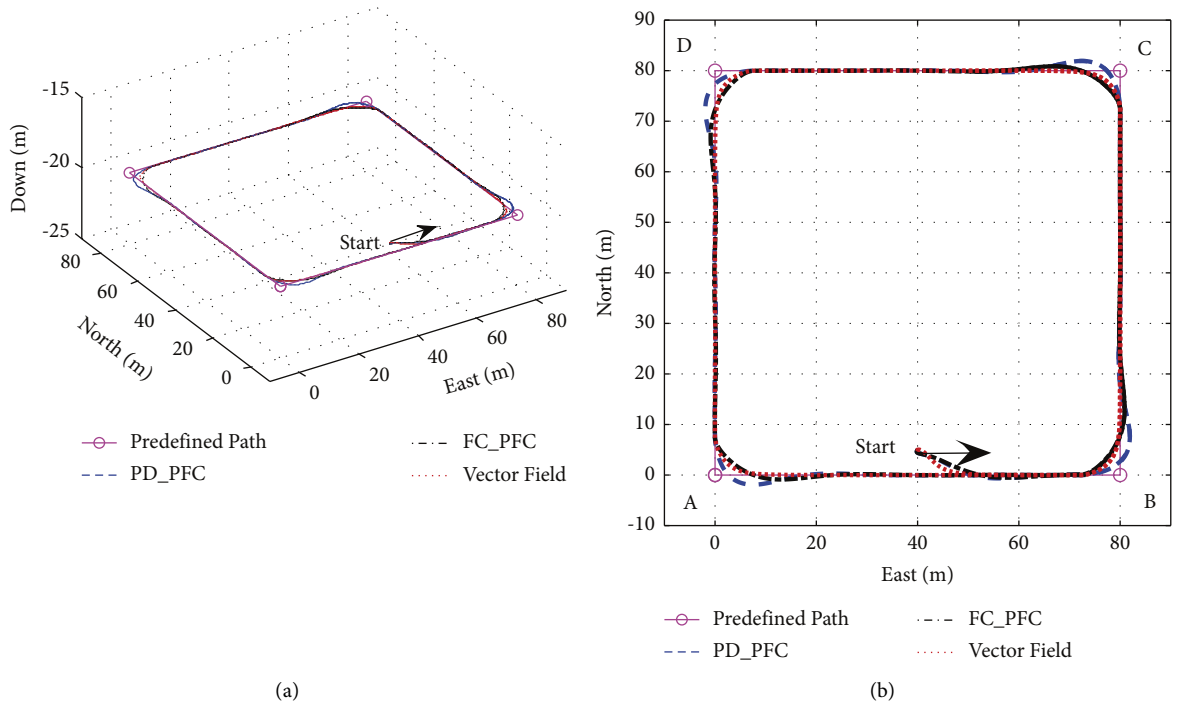

Figure 6: Comparison of the square path following with the methods PD_PFC, FC_PFC, and the vector field (a) in the north-east-down 3D frame and (b) in the horizontal plane.

method vector field is the largest. This is because almost all of the helicopter's flight is inside the square by using the method vector field. While using the methods PD_PFC and FC_PFC, the helicopter will fly across the path during its turning.

Table 3 shows the comparison of the flight time of each route with the three methods. It can be shown that the method PD_PFC will cost the most time to complete each route. Table 4 shows the comparison of the moment when the vehicle starts to turn with the three methods. It shows that the method vector field will make the helicopter switch the waypoints firstly.

It means that it takes the least time for the helicopter with the method of the vector field to reach the waypoints.

Table 3 shows the comparison of the flight time of each route with the three methods. It can be shown that the method PD_PFC will cost the most time to complete each route. Table 4 shows the comparison of the moment when the vehicle starts to turn with the three methods. It shows that the method vector field will make the helicopter switch the waypoints firstly. It means that it takes the least time for the helicopter with the method of the vector field to reach the waypoints.

The above indicates that the method vector field can achieve the best path following of the predefined square path than those by using the methods PD_PFC and FC_PFC. Although the method PD_PFC has the performance of the shortest rise time, it has the largest overshoot, convergence time, and oscillation amplitude. With the parameter K_2 adjusted by the fuzzy logic, the method FC_PFC can follow the square path better than that by using the method PD_PFC. But the design of the fuzzy rules of the method FC_PFC is limited. The fuzzy rules cannot be fully considered. It makes the FC_PFC still have a larger overshoot than those by using the method vector field. And it takes more flight time for the vehicle to reach the goal with the

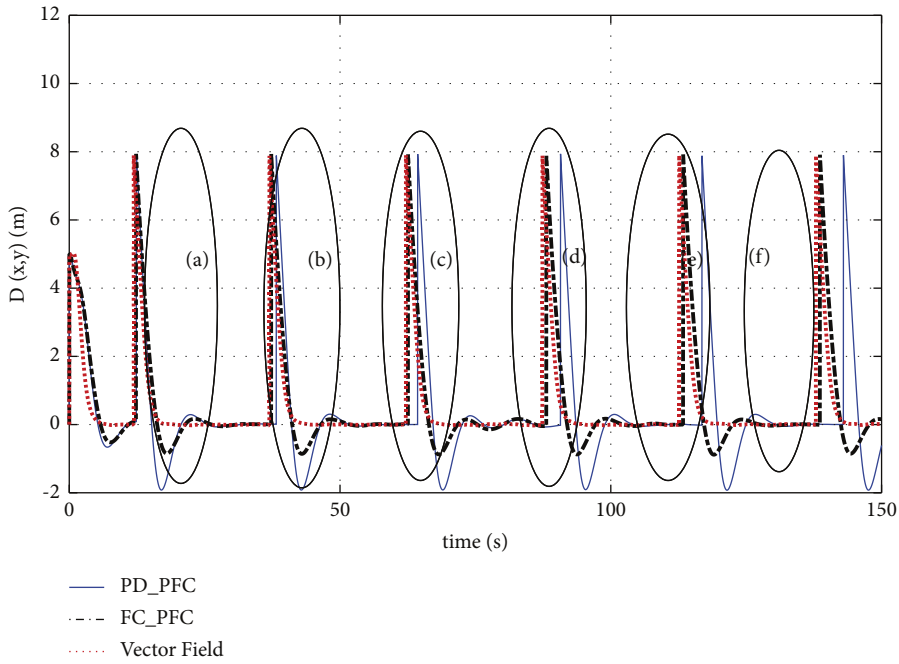

Figure 7: Comparison of the deviation $D(x, y)$ with the methods, PD_PFC, FC_PFC, and the vector field.

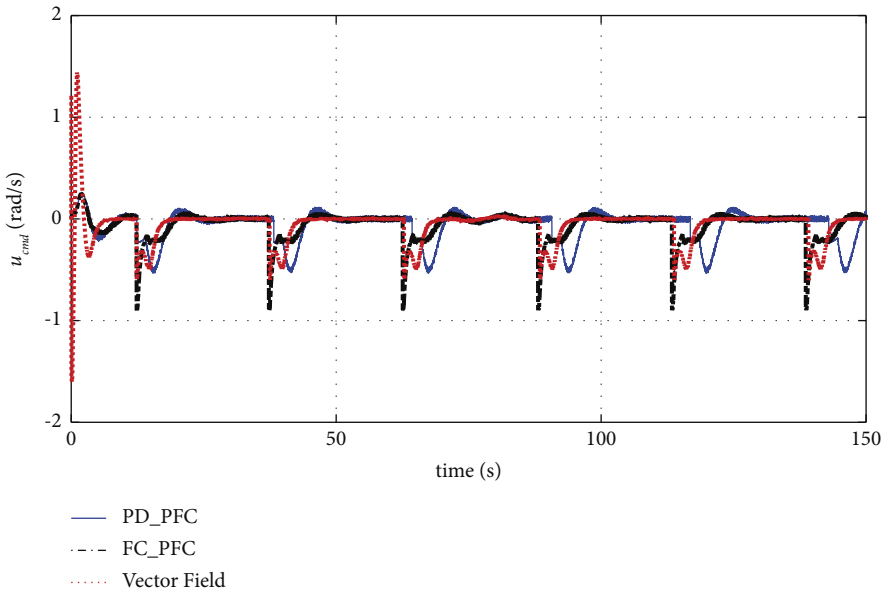

Figure 8: Comparison of u_{cmd} with the methods, PD_PFC, FC_PFC, and the vector field.

method FC_PFC than that by using the method vector field. In comparison, the control law designed by using the method vector field is based on the smooth transition to the predefined path firstly. And it makes the method vector field have the best advantage.

4.2. Quadratic and Cubic Curve Path Following. The circle and ellipse are chosen as the predefined paths in this section. The initial position of the small unmanned helicopter was set as (40, 25, −20) in the local north-east-down coordinate. The functions of the predefined circle and ellipse are $f(x, y)$: $(x - 40)^2/900 + (y - 30)^2/900 - 1 = 0$ and $f(x, y)$: $(x - 40)^2/400 + (y - 30)^2/900 - 1 = 0$, respectively. Figures 11(a) and 12(a) show that the helicopter will follow the predefined quadratic paths after the approximation of transition. Figures 11(b) and 12(b) show that the nominal distance $d(x, y)$ will approach zero with the bounded following error in finite time. Figure 11(c) shows that the course rate command generated by the method vector field will

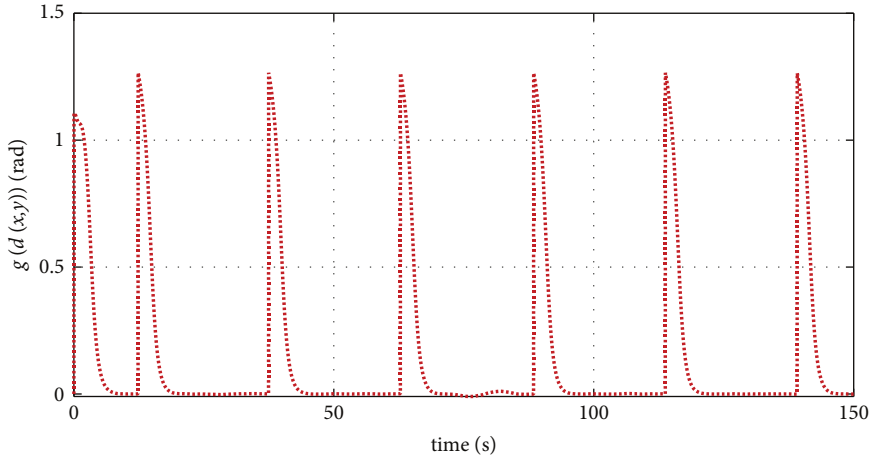

Figure 9: $g(d(x, y))$ in (3) while following the predefined square path.

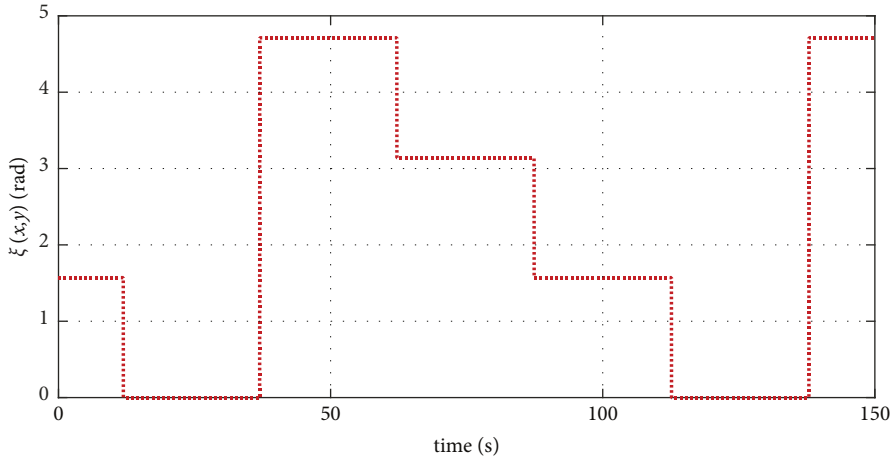

Figure 10: $\xi(x, y)$ in (3) while following the predefined square path.

Table 1: Comparison of the maximum overshoot and rise time about $D(x, y)$ with the methods the vector field, FC_PFC, and PD_PFC.

	Maximum overshoot (m)			Rise time (s)			Convergence time (s)		
	Vector field	FC_PFC	PD_PFC	Vector field	FC_PFC	PD_PFC	Vector field	FC_PFC	PD_PFC
Area (a)	−0.0134	−0.8138	−1.9197	3.66	3.54	2.64	3.66	7.64	7.38
Area (b)	−0.0060	−0.8572	−1.9187	3.66	3.50	2.64	3.66	7.64	7.36
Area (c)	−0.0147	−0.8569	−1.9161	3.67	3.51	2.66	3.67	7.72	7.38
Area (d)	−0.0134	−0.8473	−1.9073	3.65	3.49	2.66	3.65	7.66	7.36
Area (e)	−0.0152	−0.8484	−1.9238	3.70	3.52	2.63	3.70	7.64	7.34
Area (f)	−0.0131	−0.8635	−1.9217	3.70	3.45	2.64	3.70	7.64	>7.00

approach 0.1 rad/s while the helicopter is flying along the circle path with a radius of 30 meters at a speed of 3 m/s. Since the curvature of each point on the ellipse is not the same, Figure 12(c) shows that the course rate command generated for the ellipse path following varies periodically while the helicopter is flying along the ellipse round and round.

For cubic curve path following, the function of the predefined cubic curve is $f(x, y)$: $0.0005x^3 - y = 0$. The initial position of the small unmanned helicopter was set as (−30,

Table 2: Comparison of the statistical result about $D(x, y)$ with the three methods.

Method	Mean (m)	MSE (m)
Vector field	0.5778	1.5325
FC_PFC	0.5307	1.6713
PD_PFC	0.3095	1.7065

Table 3: Comparison of the flight time of each route with the three methods.

Method	The flight time of every section (s)				
	Route BC	Route CD	Route DA	Route AB	Route BC
Vector field	25.06	25.20	25.26	25.24	25.26
FC_PFC	24.96	25.26	25.54	25.26	25.26
PD_PFC	25.84	26.10	26.38	26.12	26.12

Table 4: Comparison of the moment when the vehicle starts to turn with the three methods.

Method	The moment when the vehicle starts to turn (s)					
	Area (a)	Area (b)	Area (c)	Area (d)	Area (e)	Area (f)
Vector field	11.90	36.96	62.16	87.38	112.62	137.88
FC_PFC	12.34	37.30	62.56	88.10	113.36	138.62
PD_PFC	12.40	38.24	64.34	90.72	116.84	142.96

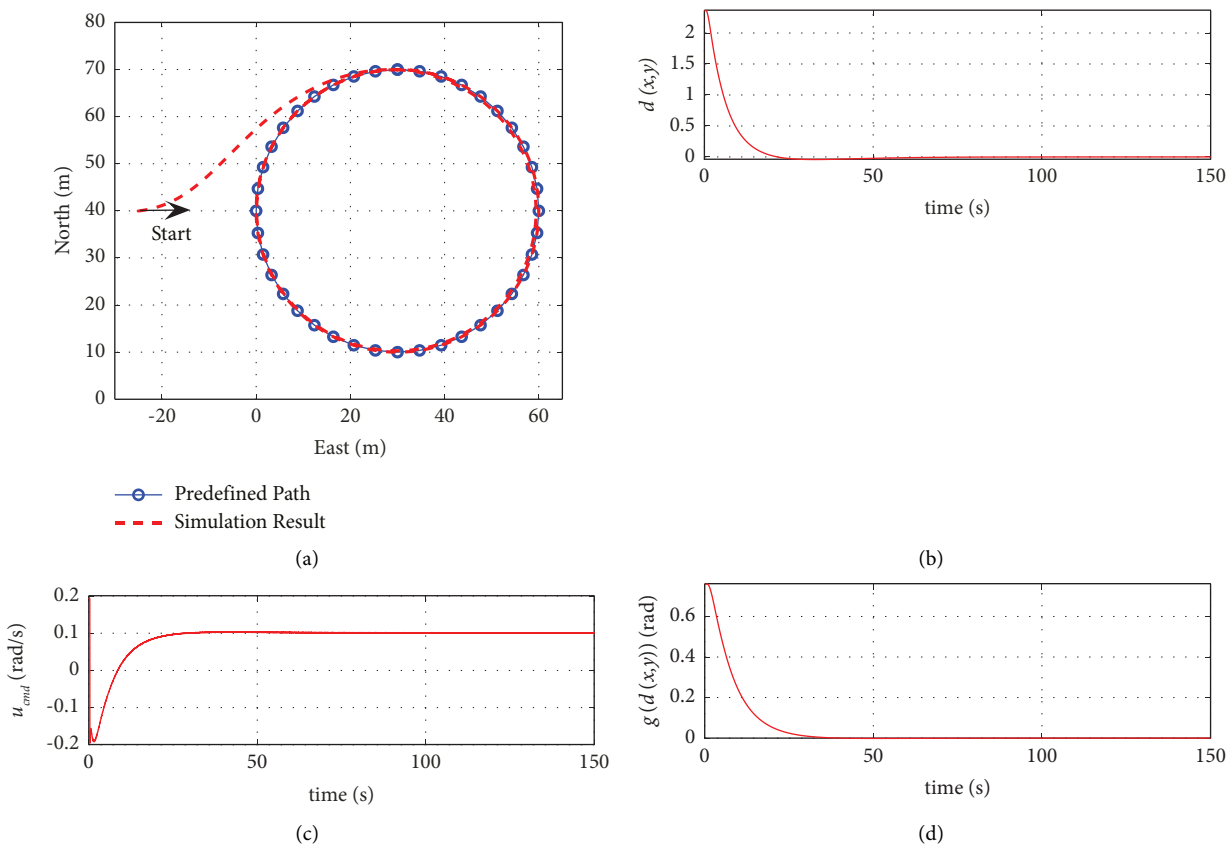

Figure 11: Continued.

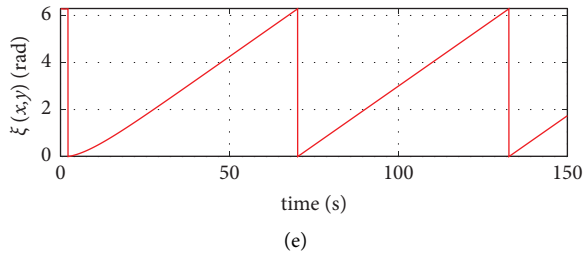

(e)

Figure 11: Simulation results of vector field-based circular path following (a) predefined and simulated flight path, (b) the nominal distance $d(x, y)$, (c) the course rate command u_{cmd}, (d) $g(d(x, y))$ in (3), and (e) $\xi(x, y)$ in (3).

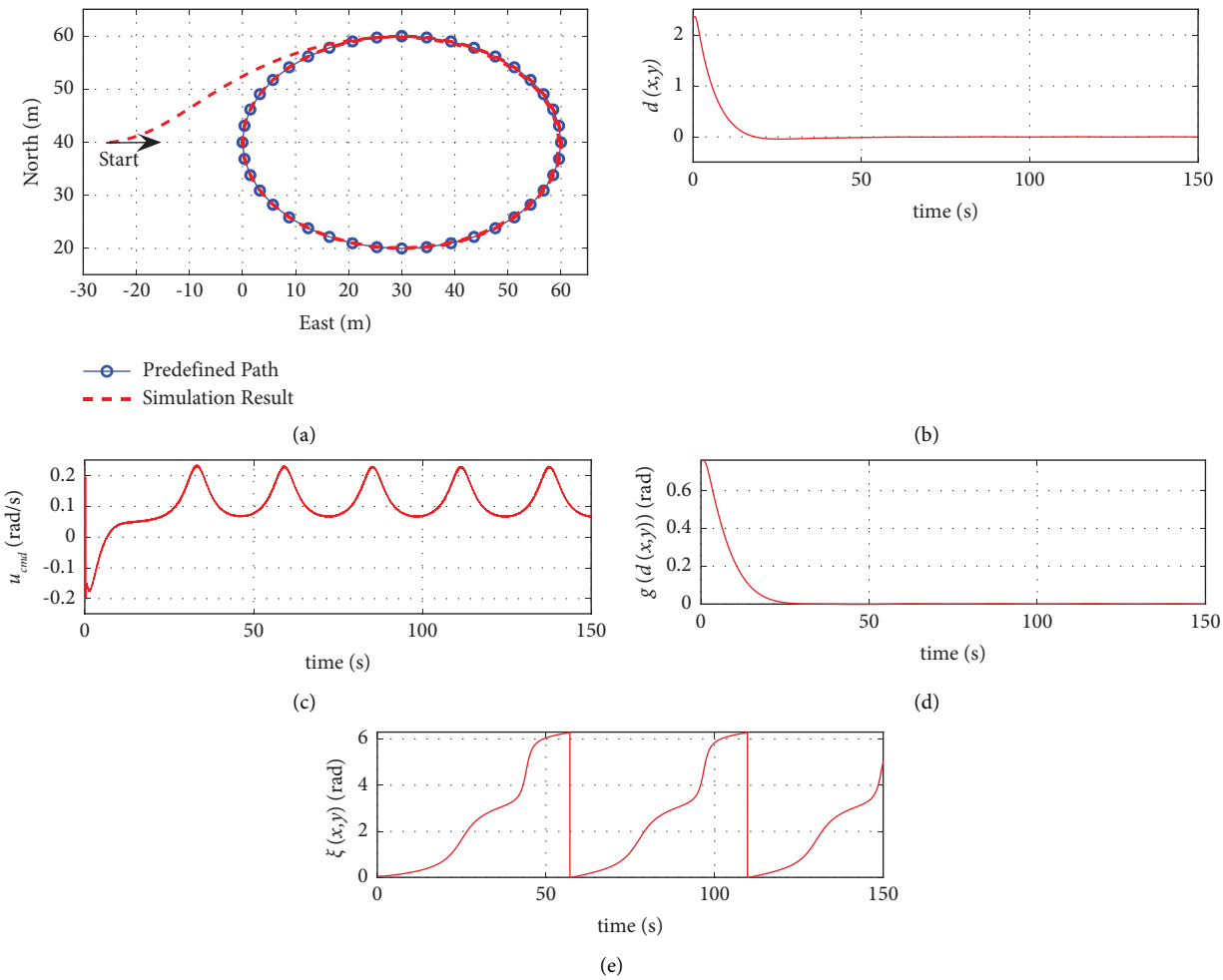

Figure 12: Simulation results of vector field-based elliptic path following (a) predefined and simulated flight path, (b) the nominal distance $d(x, y)$, (c) the course rate command u_{cmd}, (d) $g(d(x, y))$ in (3), and (e) $\xi(x, y)$ in (3).

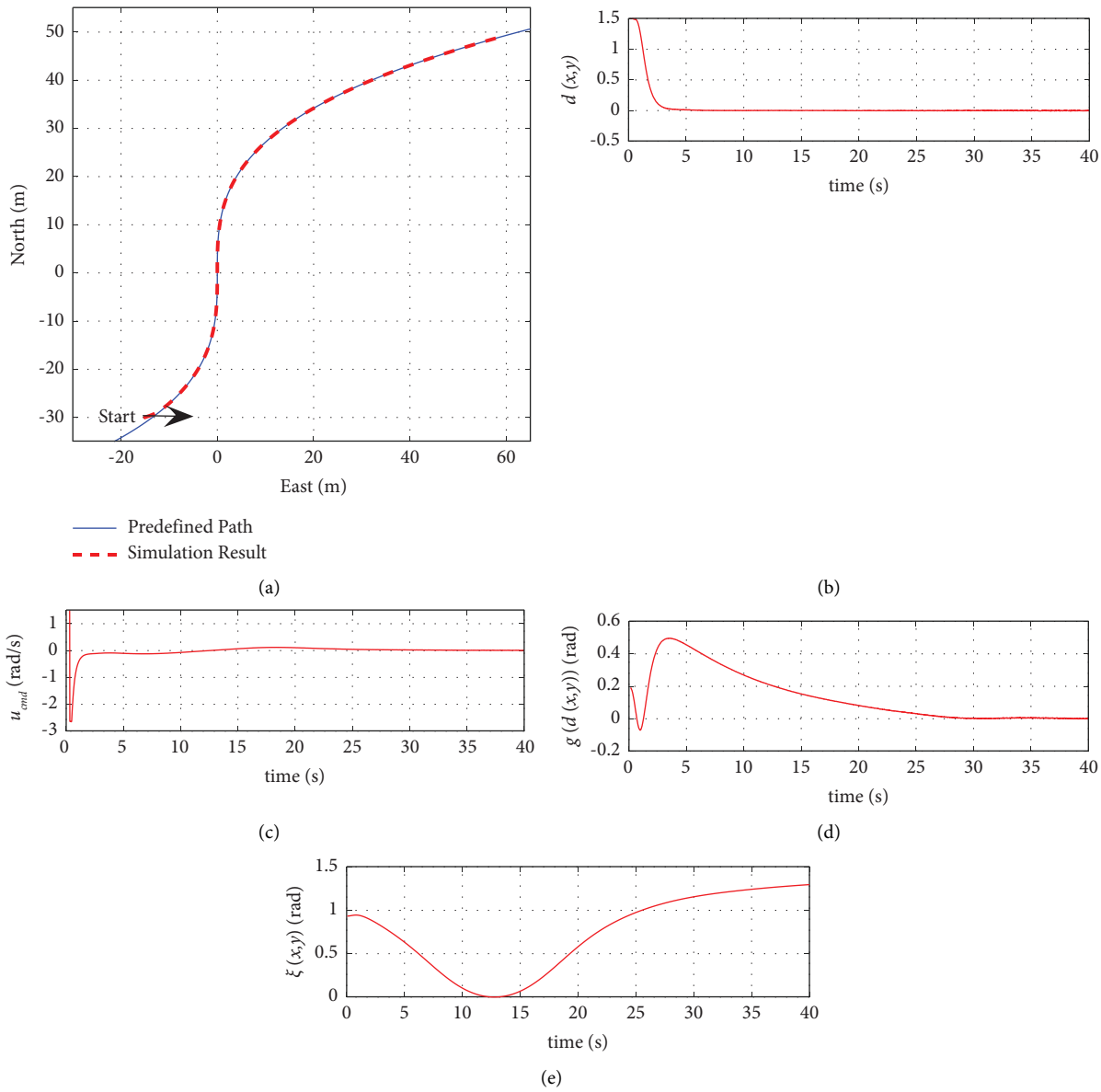

FIGURE 13: Simulation results of vector field-based cubic-curve path following (a) predefined and simulated flight path, (b) the nominal distance $d(x, y)$, (c) the course rate command u_{cmd}, (d) $g(d(x, y))$ in (3), and (e) $\xi(x, y)$ in (3).

-15, -20) in the local north-east-down coordinate. Figure 13(a) shows that the helicopter will follow the predefined cubic path after it has reach the path. The nominal distance $d(x, y)$ shown in Figure 13(b) indicates that there is no overshoot when the helicopter flies towards the cubic path.

5. Conclusions

The guidance of the helicopter to realize the horizontal desired path following has been designed based on the concept of the vector field. The guidance law only needs the inertial information of the helicopter including the position and velocity in the north-east frame and the implicit function of the desired path. The asymptotic stability analysis of the horizontal smooth path following with bounded errors has also been given. Compared with the work in [25], the flight paths have been extended to a class of the smooth curve which can be expressed by implicit functions. Compared with the work in [24], the conditions for the stability of the proposed vector field guidance method have been extended.

Simulations on following four types of planar paths, i.e., the square, circular, elliptic, and cubic curve paths, have verified the effectiveness of the proposed method. Furthermore, another two PD-like nonlinear control laws, PD_PFC and FC_PFC, were also applied to the square path following. The comparison shows that the method vector field has the best path following performance. The helicopter will arrive each waypoint and converge to the next route with the shortest arrival time by using the method vector field. Additionally, the simulation flight path produced by using

the method vector field is the smoothest with the smallest overshoot. The guidance law designed in this paper can also be applied in the guidance of UGV and other types of UAV working in the horizontal plane.

It can be found that the function $g(x)$ in (3) will influence the process that the helicopter reaches the sliding surface. In the future, a suitable function with satisfactory parameters designed will be studied to make the helicopter follow a serial of smooth paths better. Additionally, since the ground velocity in the horizontal plane V_g can vary within $[V_{g,\min}, V_{g,\max}]$, another control law to adjust the velocity V_g considering the convergence rate of different kinds of path will also be invested.

When there is external interference, especially the wind is larger enough, the assumption that the heading of the flying vehicle ψ is equal to its course χ cannot be guaranteed. In this case, the kinematic model shown as (2) is not suitable for generating the heading rate command. The kinematic model which is the function of the heading, airspeed, and wind speed [25] will be used to generate the heading rate command.

Data Availability

The labeled data used to support the findings of this study are available from the corresponding author upon request.

Conflicts of Interest

The authors declare that they have no conflicts of interest.

Acknowledgments

This work was supported by the National Natural Science Foundation of China (grant no. 61503172), the Natural Science Foundation of Fujian Province (grant no. 2020J05197), and the Shenzhen Special Funds for the Construction of High-Level Universities (grant no. 02326402).

References

[1] X. Wang, S. Baldi, X. Feng, C. Wu, H. Xie, and B. De Schutter, "A fixed-wing UAV formation algorithm based on vector field guidance," *IEEE Transactions on Automation Science and Engineering*, vol. 20, no. 1, pp. 179–192, 2023.

[2] S. Islam, X. P. Liu, and A. E. Saddik, "Adaptive sliding mode control of unmanned four rotor flying vehicle," *International Journal of Robotics and Automation*, vol. 30, no. 2, pp. 140–148, 2015.

[3] B. Xian, X. Zhang, H. Zhang, and X. Gu, "Robust adaptive control for a small unmanned helicopter using reinforcement learning," *IEEE Transactions on Neural Networks and Learning Systems*, vol. 33, no. 12, pp. 7589–7597, 2022.

[4] G. Chowdhary, E. N. Johnson, D. Magree, A. Wu, and A. Shein, "GPS-denied indoor and outdoor monocular vision aided navigation and control of unmanned aircraft," *Journal of Field Robotics*, vol. 30, no. 3, pp. 415–438, 2013.

[5] S. Zhao, Z. Hu, M. Yin et al., "A robust real-time vision system for autonomous cargo transfer by an unmanned helicopter," *IEEE Transactions on Industrial Electronics*, vol. 62, no. 2, pp. 1210–1219, 2015.

[6] D. H. Shim, H. Chung, and S. Sastry, "Conflict-free navigation in unknown urban environments," *IEEE Robotics and Automation Magazine*, vol. 13, no. 3, pp. 27–33, 2006.

[7] R. P. Padhy, F. Xia, S. K. Choudhury, P. K. Sa, and S. Bakshi, "Monocular vision aided autonomous UAV navigation in indoor corridor environments," *IEEE Transactions on Sustainable Computing*, vol. 4, no. 1, pp. 96–108, 2019.

[8] H. Yang, B. Jiang, H. Yang, and H. H. T. Liu, "Fault-tolerant cooperative control for multiple vehicle systems based on topology reconfiguration," *IEEE Transactions on Cybernetics*, vol. 52, no. 7, pp. 6649–6661, 2022.

[9] B. Zhou, X. Lu, S. Tang, and Z. Zheng, "Nonlinear system identification and trajectory tracking control for a flybarless unmanned helicopter: theory and experiment," *Nonlinear Dynamics*, vol. 96, no. 4, pp. 2307–2326, 2019.

[10] A. Razzaghian and R. Kardehi Moghaddam, "Adaptive fuzzy sliding mode control for a model-scaled unmanned helicopter," *Journal of Fuzzy Set Valued Analysis*, vol. 2016, no. 3, pp. 286–302, 2016.

[11] C. C. Tsai, C. T. Lee, and K. S. Hwang, "Intelligent adaptive trajectory tracking control using fuzzy basis function networks for an autonomous small-scale helicopter," in *Proceedings of the IEEE Conference on Systems, Man, and Cybernetics*, pp. 2255–2260, Anchorage, AK, USA, October 2011.

[12] C. C. Tsai, Z. C. Wang, C. T. Lee, and Y. Y. Li, "Intelligent adaptive trajectory tracking control for an autonomous small-scale helicopter using fuzzy basis function networks," *Asian Journal of Control*, vol. 17, no. 1, pp. 234–245, 2014.

[13] J. G. Benitez-Morales, H. Rodriguez-Cortes, and R. Castro-Linares, "A new nonlinear controller for trajectory tracking of the longitudinal dynamics of a small scale helicopter," *Journal of Intelligent and Robotic Systems*, vol. 73, no. 1-4, pp. 99–121, 2014.

[14] H. J. Kim and D. H. Shim, "A flight control system for aerial robots: algorithms and experiments," *Control Engineering Practice*, vol. 11, no. 12, pp. 1389–1400, 2003.

[15] K. Yang, S. K. Gan, and S. Sukkarieh, "An efficient path planning and control algorithm for RUAV's in unknown and cluttered environments," *Journal of Intelligent and Robotic Systems*, vol. 57, no. 1–4, pp. 101–122, 2010.

[16] B. Mettler, T. Tanade, M. B. Tischler, and W. Messner, *Attitude control optimization for a small-scale unmanned helicopter,*American Institute Of Aeronautics And Astronautics, Reston, VA, USA, 2000.

[17] B. Godbolt and A. F. Lynch, "Model-based helicopter UAV control: experimental results," *Journal of Intelligent and Robotic Systems*, vol. 73, no. 1–4, pp. 19–31, 2013.

[18] E. N. Sanchez, H. M. Becerra, and C. M. Velez, "Combining fuzzy, PID and regulation control for an autonomous mini-helicopter," *Information Sciences*, vol. 177, no. 10, pp. 1999–2022, 2007.

[19] J. Shin, K. Nonami, D. Fujiwara, and K. Hazawa, "Model-based optimal attitude and positioning control of small-scale unmanned helicopter," *Robotica*, vol. 23, no. 1, pp. 51–63, 2005.

[20] M. Bergerman, O. Amidi, J. R. Miller, N. Vallidis, and T. Dudek, "Cascaded Position and Heading Control of a Robotic Helicopter," in *Proceedings of the 2007 IEEE/RSJ International Conference on Intelligent Robots and Systems*, pp. 135–140, San Diego, CA, USA, October 2007.

[21] G. Cai, B. M. Chen, X. Dong, and T. H. Lee, "Design and implementation of a robust and nonlinear flight control system for an unmanned helicopter," *Mechatronics*, vol. 21, no. 5, pp. 803–820, 2011.

[22] P. Marantos, C. P. Bechlioulis, and K. J. Kyriakopoulos, "Robust trajectory tracking control for small-scale unmanned helicopters with model uncertainties," *IEEE Transactions on Control Systems Technology*, vol. 25, no. 6, pp. 2010–2021, 2017.

[23] X. Ma and W. Huo, "Singularity-free path following control for miniature unmanned helicopters," *Lecture Notes in Electrical Engineering*, vol. 460, pp. 669–683, 2108.

[24] T. M. Wang, J. Liang, C. Wang, Y. Zhang, and Y. Chen, "Combined of vector field and linear quadratic Gaussian for the path following of a small unmanned helicopter," *IET Control Theory & Applications*, vol. 6, no. 17, pp. 2696–2703, 2012.

[25] D. R. Nelson, D. B. Barber, T. W. McLain, and R. W. Beard, "Vector field path following for miniature air vehicles," *IEEE Transactions on Robotics*, vol. 23, no. 3, pp. 519–529, 2007.

[26] H. Yu, R. W. Beard, and J. Byrne, "Vision-based navigation frame mapping and planning for collision avoidance for miniature air vehicles," *Control Engineering Practice*, vol. 18, no. 7, pp. 824–836, 2010.

[27] H. Yu and R. W. Beard, "A vision-based three-tiered path planning and collision avoidance scheme for miniature air vehicles," *International Journal of Robotics and Automation*, vol. 30, no. 5, pp. 429–440, 2015.

[28] H. K. Khalil, *Nonlinear Systems*, Prentice-Hall, Hoboken, NJ, USA, 3 edition, 2002.

[29] Y. Chen, T. M. Wang, J. H. Liang, C. L. Wang, and C. H. Xue, "A fuzzy robust path following controller for a small unmanned air vehicle," in *Proceedings of the 2012 IEEE Conference on Industrial Electronics and Applications*, pp. 1189–1194, Singapore, July 2012.